Geopersia 2023, 13(2): 365-384
DOI: 10.22059/GEOPE.2023.356473.648707

RESEARCH PAPER

# Natural fractures in the Upper Sarvak Formation in the Lurestan Zone, the Zagros Basin, Iran

**Moosa Esfandyari [1], Hassan Mohseni [1,*], Mojtaba Heidari [1], Asghar Seif [2]**

[1] Department of Geology, Faculty of Basic Sciences, Bu-Ali Sina University, Hamedan, Iran
[2] Department of Statistics, Faculty of Basic Sciences, Bu-Ali Sina University, Hamedan, Iran

Received: 13 March 2023, Revised: 12 May 2023, Accepted: 02 June 2023


**Abstract**
Two surface sections of the Sarvak Formation in the Lurestan zone (Zagros Fold-Thrust Belt) were examined to inspect the naturally occurring fractures. The inspected sections are located in the Surgah anticline and the Kuh-e-Charmi anticline; in the Ilam and the Kermanshah provinces respectively. The Sarvak Formation was carefully examined to record the fracture types, their spatial distribution, spacing and cross-cutting relationships. Detailed examinations were undertaken on 420 fractures, 40 core plugs porosity and P-wave velocity and 205 thin sections. Three genetic types of fractures including tectonic, pressure-solution and dissolution related fractures were identified. The tectonic related fractures include two main sets (namely, with NW-SE and NE-SW trends). In addition, two types of stylolites including the bed-perpendicular and the tectonic stylolites (bed-parallel); were distinguished that postdate the fractures (veins). The Sarvak Formation underwent various diagenetic processes in couple with fracturing. The pore types include microporosity, intergranular porosity, moldic porosity and fracture-stylolite. Petrophysical measurements (performed on some core plugs prepared from surface block samples), show that the carbonates of the Sarvak Formation have low porosity (more than 74% of the samples have less than 3%) and thereby high compressional wave velocity (Vp), (more than 96% of the samples have 6000 m/s), Therefore, it could be concluded that the Sarvak Formation is a tight interval in a reservoir aspect.

**Keywords:** The Sarvak Formation, Zagros Basin, Fractured Reservoir.

## Introduction

More than 60% of the world's oil and 40% of the world's gas reserves are trapped in the carbonate reservoirs (Lee et al., 2015). The Zagros Fold-Thrust Belt (ZFTB) contains nearly half of the world's hydrocarbon reserves (Cooper, 2007). Hydrocarbons are mainly stored in the Mesozoic and Cenozoic carbonates (Bordenave, 2008), which are severely fractured due to regional tectonic activities, and the majority of hydrocarbon production is dependent on these fractures (Kosari et al., 2017). Naturally fractured reservoirs are very important, since the fractures/joints systems could considerably enhance the reservoir quality via improving the permeability (Warren, 2006; Van der Voet et al., 2020). Analysis of fractures is an essential task for understanding the heterogeneities of carbonate reservoirs, since they could significantly control the reservoir quality, particularly porosity and permeability (Lavenu et al., 2015). Each set of fractures in a reservoir has its own individual characteristics (geometry, aperture, spacing, distribution, connectivity, and hydraulic characteristics), which either can enhance or reduce the reservoir quality (Aydin, 2000). Hence, investigating and identifying the fracture networks

* Corresponding author e-mail: mohseni@basu.ac.ir

in the carbonate reservoirs is an important challenge for hydrocarbon exploration and production (Lavenu et al., 2015; Kosari et al., 2017; Tavani et al., 2018); as they are extremely heterogeneous from pore to field scale (Barbier et al., 2012).

Understanding the spatial distribution of fractures in the reservoirs is necessary to identify potential pathways of fluid flow and hydrocarbon migration (Barbier et al., 2012). Fracture organization is essential for understanding the fluid flow in the carbonate rocks, as they act as key parameters in tight, non-porous carbonate intervals (Lavenu et al., 2015). Fluid accumulation and flow in the fractured reservoirs could occur in two systems, including fractures and matrix; as a result, characteristics of the both media must be evaluated (Kosari et al., 2017). The physical characteristics of fractures are controlled by their generation, mechanical characteristics and diagenetic processes of the host rock, because they could enhance or decrease the porosity and permeability (Nelson, 2001).

Inspecting the fractures on the outcrops could facilitates to achieve a better understanding of their 3-D patterns, and distribution (Lavenu et al., 2015). Subsurface data i.e., core plugs, and well loges do not provide sufficient information neither for describing the fracture network and geometry, nor for their spatial pattern (Angerer et al., 2003; Lynn, 2004). Limitations arise from relatively small scale, and low resolution, thus they do not enable us to establish a relationship between one-dimensional and 3-D models and to predict a realistic 3-D model (Angerer et al., 2003; Peacock, 2006). Whereas, in the outcrops, the factors controlling the pattern of fractures can be easily investigated.

Despite the vital role of natural fractures on the reservoir quality of the carbonate reservoirs, it is still an emerging task. A plenty of literature are available discussing about the distribution of fractures in the Zagros Basin (e.g., Wennberg et al., 2006; 2007; Ahmadhadi et al., 2008; Cassini et al., 2011; Awdal et al., 2013; Carminati et al., 2013, 2014; Kothari et al., 2017; Tavani et al., 2018). Yet, their genesis and development and their contribution to the reservoir performance are less understood. The main goal of this research is to inspect natural fractures and understand their possible role on the reservoir performance of the Sarvak Formation in the Lurestan Zone in the Zagros Basin.

## Geological setting

The Zagros Mountain range is the consequence of a complex multi-stage geodynamic evolution that affected the eastern margin of the Arabian Plate since late Cretaceous (Vincent et al., 2015). These stages include the platform setting during the Paleozoic; the Tethys widening stage in Permian-Triassic; formation of passive continental margins followed by a prolonged period of stable, shallow marine environments (with the see floor spreading towards the northeast) during Jurassic-early Cretaceous, the Neo-Tethys oceanic crust subduction in the late Cretaceous; and finally, the closure of the Neo-Tethys and the deformation of the foreland in the late Miocene (Berberian and King, 1981; Alavi, 1991; 2007; Agard et al., 2005; Verges et al., 2011). By closure of the Neo-Tethys back-arc basins, the remnant of Neo-Tethys Ocean persisted as a relatively narrow fore-arc basin, where the upper Cretaceous to upper Miocene sediments were deposited (Kordi, 2019).

The ZFTB is located on the northern margin of the Arabian Plate (Berberian and King, 1981). It was divided into several morphotectonic zones (Falcon, 1961; Berberian, 1995), which are bounded by deep basement faults (Falcon, 1974; Berberian, 1995). Among them the simple fold belt has a chain of folds comprising thick Paleozoic to Cenozoic sediments (about 10-13 km) accumulated on the northern margin of the Arabian Plate (Farzipour-Saein et al., 2009). They are limited by the high Zagros Fault and the Mountain Front Fault toward NE and SW respectively (Casciello et al., 2009). The ZFTB includes several sub-basins including the Dezful Embayment and the Lurestan Zone (Motiei, 1993) (Fig. 1).

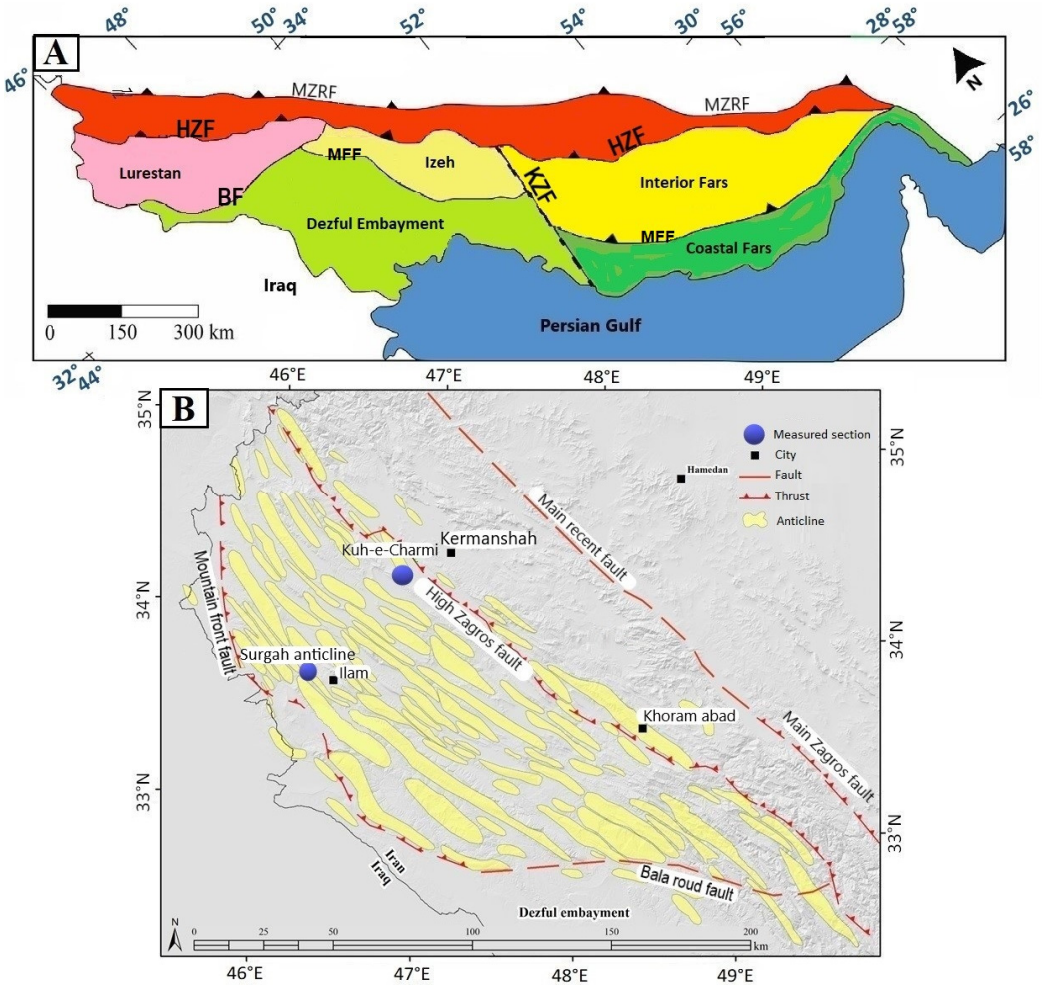


**Figure 1.** Location and geological map of the study area, A: Subdivision zones of the ZFTB (modified after-Saein et al., 2009), B: location map of Lurestan zone with its main structures with location of the study sections. HZF=High Zagros Fault, MZRF=Main Zagros Reverse Fault, KZF=Kazeron Fault, BF=Bala roud Fault, MFF=Mountain Front Fault

A succession of shallow-marine carbonates with subordinate evaporites were accumulated in the basin from late Triassic to late Cretaceous that are intercalated with siliciclastics (Heydari, 2008). The organic-rich deep-water deposits of the Gadvan and Garau formations were deposited during relative sea level rise (Setudehnia, 1978). Probably, a short relative sea level fall occurred at the end of the sedimentation of the Dariyan Formation, succeeded by a relative sea level rise, which promoted the accumulation of organic rich marine sediments of the Kazhdumi Formation; followed by the Sarvak Formation (Heydari, 2008).

The Sarvak Formation was inspected in the Lurestan Zone (Kuh-e-Charmi and Surgah anticlines) (Figures 1B and 2). In this zone, the Mesozoic-Cenozoic succession consists of about 4-5 km of pre-orogenic and 4-5 km of syn-orogenic sediments (Homke et al., 2009). The pre-orogenic Mesozoic succession is mainly composed of carbonate units, which includes the Garau, Sarvak, Surgah, Ilam, Gurpi and Pabdeh formations and syn-orogenic sediments includes the Amiran-Kashkan clastic succession, Shahbazan-Asmari shallow marine carbonates, the Gachsaran evaporitic Formation and the Aghajari and Bakhtiari siliciclastics (Homke et al., 2009). The Lurestan Zone has a long history of hydrocarbon exploration and production, (Farzipour-Saein et al., 2009); where effective source rocks, seals and carbonates reservoirs were accumulated of which the Sarvak Formation is of a particular interest (Motiei,

1993).

## Materials and methods

A total of 205 samples of the Upper Sarvak Formation in the Lurestan Zone of the Zagros Basin in west of Iran, were collected from two outcrops for facies analysis, pore typing and petrographic analysis. In the both of inspected outcrops, only the upper part of the Sarvak Formation is exposed that experienced identical tectonic events and diagenetic processes. In each outcrop, thickness of the layers was measured and sedimentary textures were described (Dunham, 1962). A further 40 samples (plugs) were also examined for petrophysical measurements (P-wave velocity and porosity). P wave velocity was measured on plugs with a diameter of 5.08cm (2in.). The pulse transmission method (Birch, 1960) was used to determine the P wave velocity for dry samples under atmospheric pressure and temperature conditions. The P-wave velocity calculation was based on equation 1:

$$V_p = d/\Delta t \quad (1)$$

where d is the length of the plug (in cm) and Δt is the P-wave interval travel time measured through the plug (μs).

The plugs, porosity (40 sample) was measured by using helium pycnometry method (in APEX Technologies Co. Arak, Iran) which was based on gas expansion principles (Boyle-Mariotte law) and could be calculated using the equation 2:

$$V_p = V_b - V_g \quad (2)$$

where $V_p$ is the plug pore volume, $V_b$ is the plug bulk volume, $V_g$ is the plug matrix volume.

Fracture attitudes including strike, height, spacing, opening, fracture density, type of appearance or complication (seams, veins and stylolite), infill materials (e.g., calcite or dolomite) and abutting relationships with bedding and cross-cutting relationships between the fracture sets were recorded. The fracture spacing was calculated based on the fracture density by using Terzaghi's (1965) rules. Fracture frequency were recorded per length unit along a line perpendicular to each fracture set and orientation. The cross-cutting relationships, texture and nature of fracture filling were also recorded for each individual fracture and fracture set. The fracture density refers to the linear density that was measured based on the number of fractures per unit length. The height of fractures was measured for the studied sections and also in each layer. Fracture orientations were measured with a compass and were plotted on a stereograph to prepare rose diagrams.

## Results

### *Fracture characteristics*

Three main types of natural fractures, including tectonic, pressure solution and dissolution fractures were identified, among which tectonic fractures are more common than the other ones.

#### Tectonic fractures

Statistical analysis of tectonic fractures of the studied surface sections revealed that they were are developed in two main sets with NW-SE and NE-SW strikes (Fig. 3); and their pattern and occurrences are relatively constant. Their trend and high dihedral angle (i.e., 90°-110°) suggest that the two sets are actually inherited joints (Tavani et al., 2018). On the cross-section, tectonic fractures may pass through the layers of Sarvak Formation and have a height of the several meters height (Figure 4A). Although, many of these tectonic fractures with up to less than a few decimeters and are limited to the bedding planes (Fig. 4B). On the horizontal plane, tectonic fractures show mutual cross-cutting relations with each other (cut through or arrest each other)

and their length varies from several centimeters to a few tens of centimeters (Fig. 4C).

More than 60% of the tectonic fractures are open-mod (Figs. 4 and 5D), while the rest are completely or partially filled with calcite and dolomite (Figs. 5A-C).

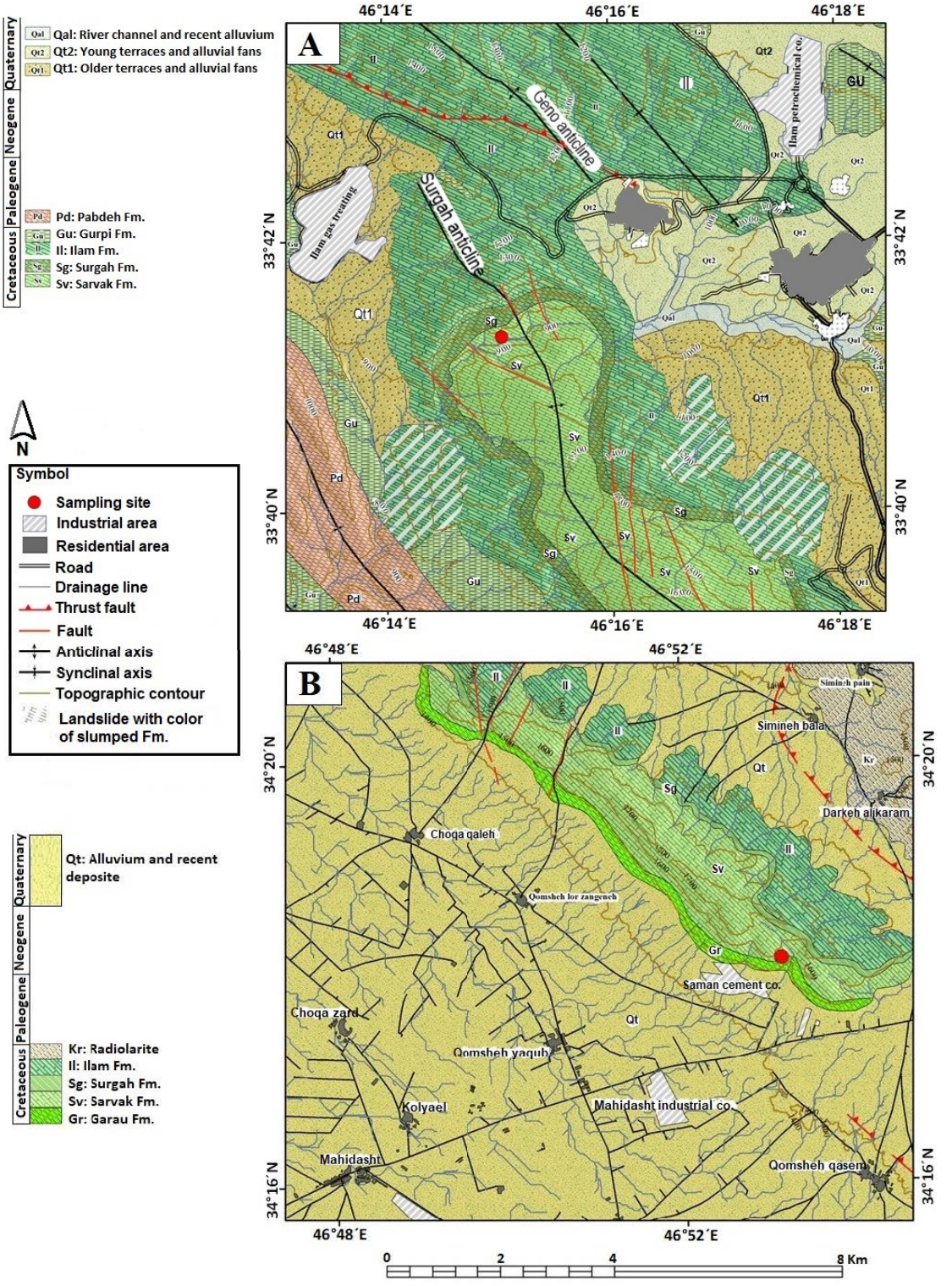


**Figure 2.** Location and geological map of the studied sections, A: Surgah anticline in the Ilam province, B: Kuh-e-Charmi section in the Kermanshah province

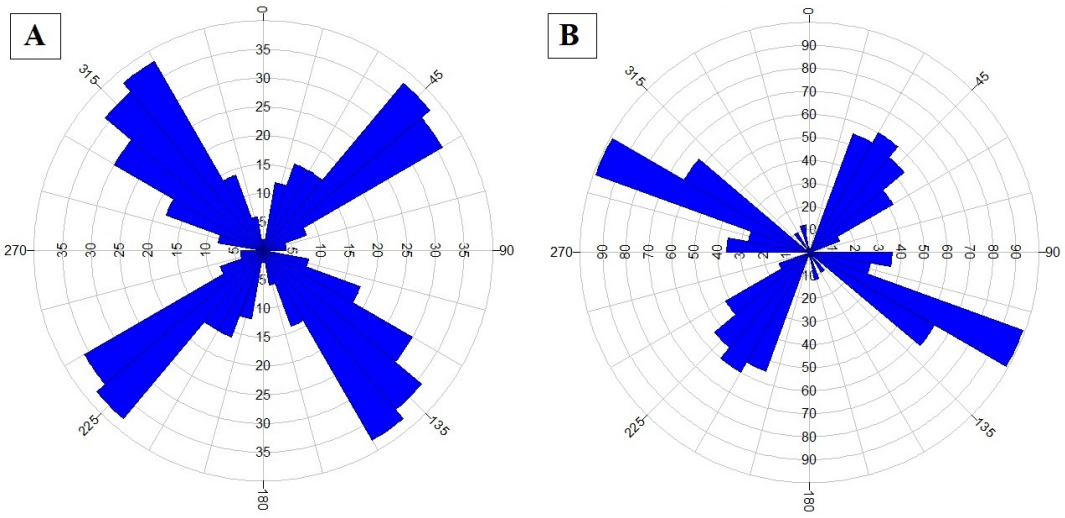


**Figure 3.** Rose diagrams showing the orientations of tectonic fractures in the outcrops of the Sarvak Formation in the Lurestan Zone, A: in the Kuh-e-Charmi section and B: in the Surgah anticline

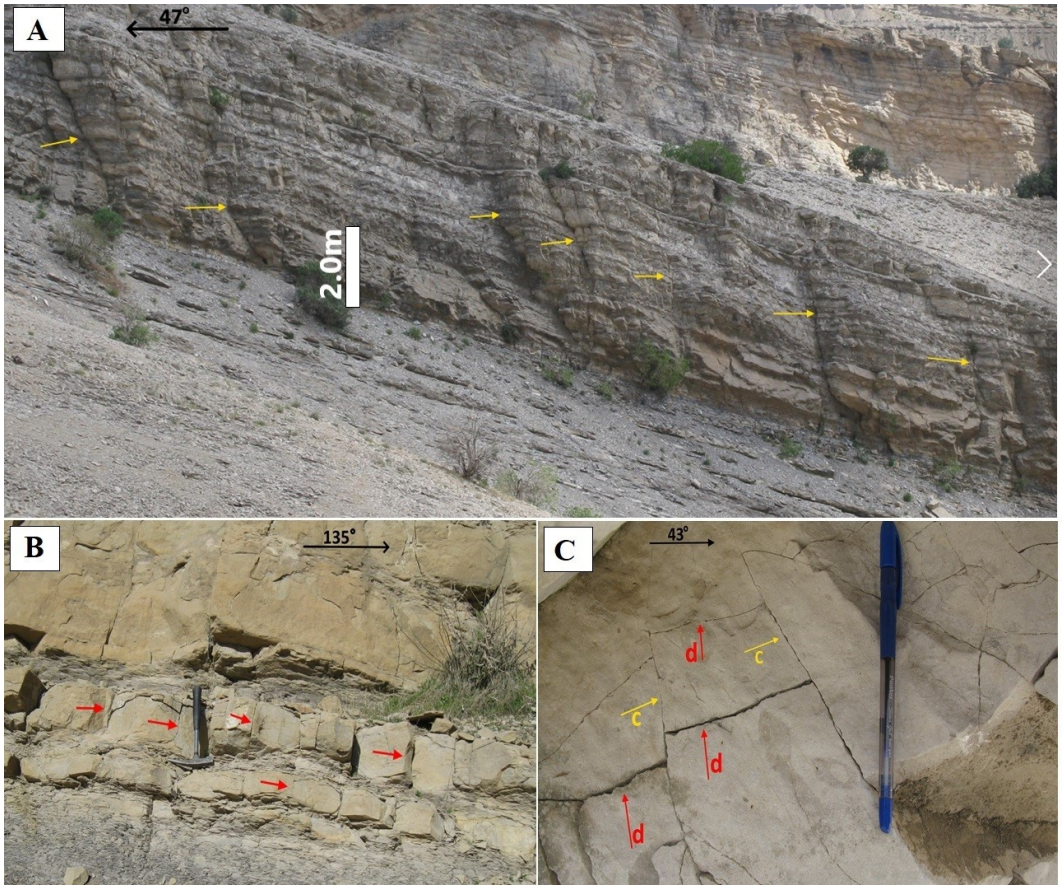


**Figure 4.** Tectonic fractures in studied outcrops, A: Fractures with a height of several meters, B: fractures with a height of several decimeters through layers, C: a set of fractures with cross-cutting relationships, note where the set c offsets the set d

Microscopic examination of thin sections showed that tectonic fractures are widespread in the Sarvak Formation (Fig. 6). Two sets of tectonic fractures cut across or join together (Fig. 6A) to make a mesh network (Fig. 6B) are common.

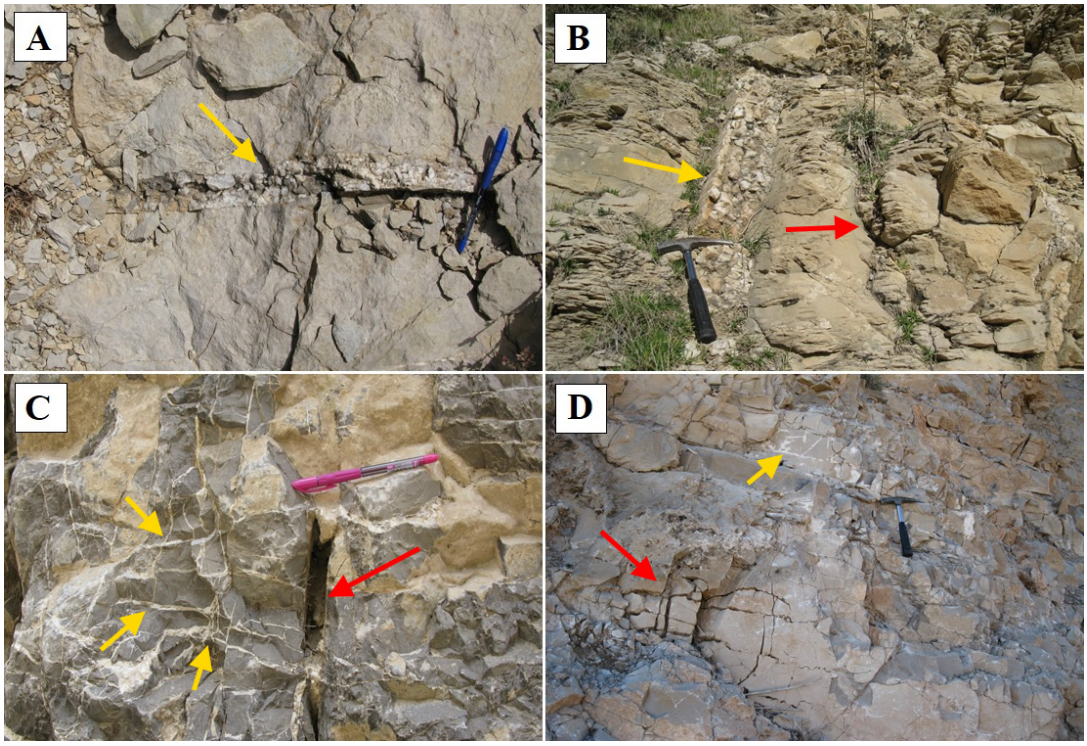


**Figure 5.** Outcrops image of tectonic fractures, A and B: fractures filled with calcite (yellow arrow), C and D: a mesh of network of the fractures filled with calcite (yellow arrow) and an open-mod fracture (red arrow)

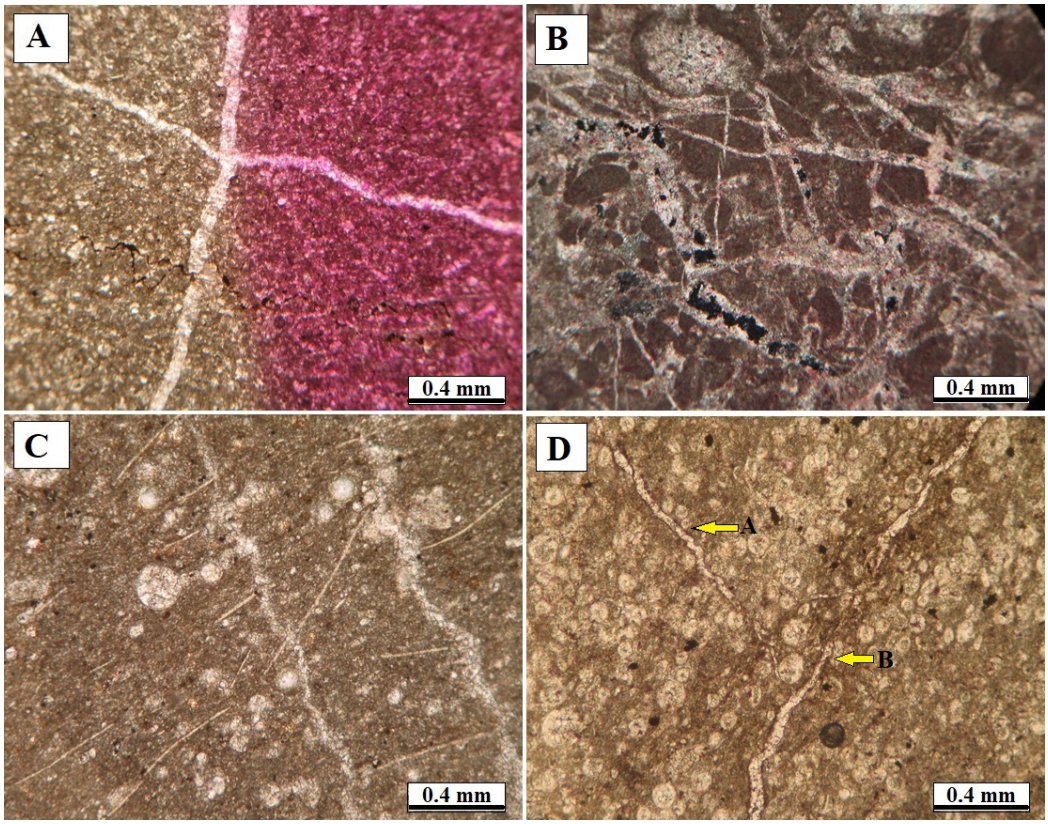


**Figure 6.** Tectonic fractures in thin sections, A: fractures that cut each other, B: fractures that formed a network, C: parallel fractures and D: Fractures that arrest each other (B type terminates A type)

Less than 40% of tectonic fractures are open on thin section observations (Fig. 6B). Their aperture is different, most have a range of 60 to 100μm. Some sets of fractures are parallel (Fig. 6C), whereas the others, arrest each other (Fig. 6D).

Pressure solution fractures

These types of fractures were developed under burial diagenesis and tectonic processes caused by pressure solution (Dunham and Larter, 1981). They are important in various aspects including: 1; they indicate the degree of chemical compaction or shortening of a rock (Petit and Mattauer, 1995), 2; they can be used to calculate the overburden or tectonic stress (Ebner et al., 2010; Beaudoin et al., 2016), 3; they can act either as fluid flow unit or barrier and therefore can drastically control the permeability distribution of rocks (Al-Sharhan and Sadd, 2000).
Stylolites are the most obvious product of the pressure solution in the carbonates. At the outcrop scale, stylolites are rough planes that collect relatively insoluble materials with different characteristics compared to the host rock and cause the anisotropy of the host rock (Koehn et al., 2016). Diagenetic stylolites that are parallel to the bedding plane (Koehn et al., 2016), and can be identified by features that bending, discontinuity, and branching (Liu et al., 2020), in contrast to the, tectonic stylolites are normal to the bedding plane (Kohen et al., 2016).

Both types of parallel to the bedding plane and the tectonic stylolites were observed in the Sarvak Formation. The amplitudes of the bedding-parallel stylolites are perpendicular to the bedding plane, which indicates their were originated by the maximum paleo-stress direction perpendicular to the bedding (Nelson, 1981). This feature was likely developed during burial diagenesis and is very common in the Sarvak Formation (Fig. 7). On the other hand, tectonic stylolites are perpendicular or oblique to the bedding and have horizontal crests (Fig. 7), that indicate their development due to maximum horizontal stress (Liu et al., 2020). Although, this type is uncommon and was exclusively observed in the fine-grained facies, particularly in the mud matrix.


**Figure 7.** Stylolites in the outcrop, bedding plane (red arrow), bedding-parallel stylolites (yellow arrows) and perpendicular to bedding plane stylolites (black arrow)

**Dissolution fractures**

Once the dissolution fractures are formed, their walls are rough and uneven (Fig. 8). Dissolution fractures, which are formed by connecting several pores like a string of beads, are expected to act as reservoir effective storage spaces for hydrocarbons (Liu et al., 2020). Sometimes the remnants of the original pore spaces could be recognized. Additionally, mineral-filled fractures can also evolve to dissolution fractures, when unstable infill minerals are completely or partially removed due to reaction with acidic fluids or groundwater leaching (Fig. 8C). In general, dissolution fractures have an irregular shape, often spiral-like and anastomosing (Rustichelli et al., 2012).

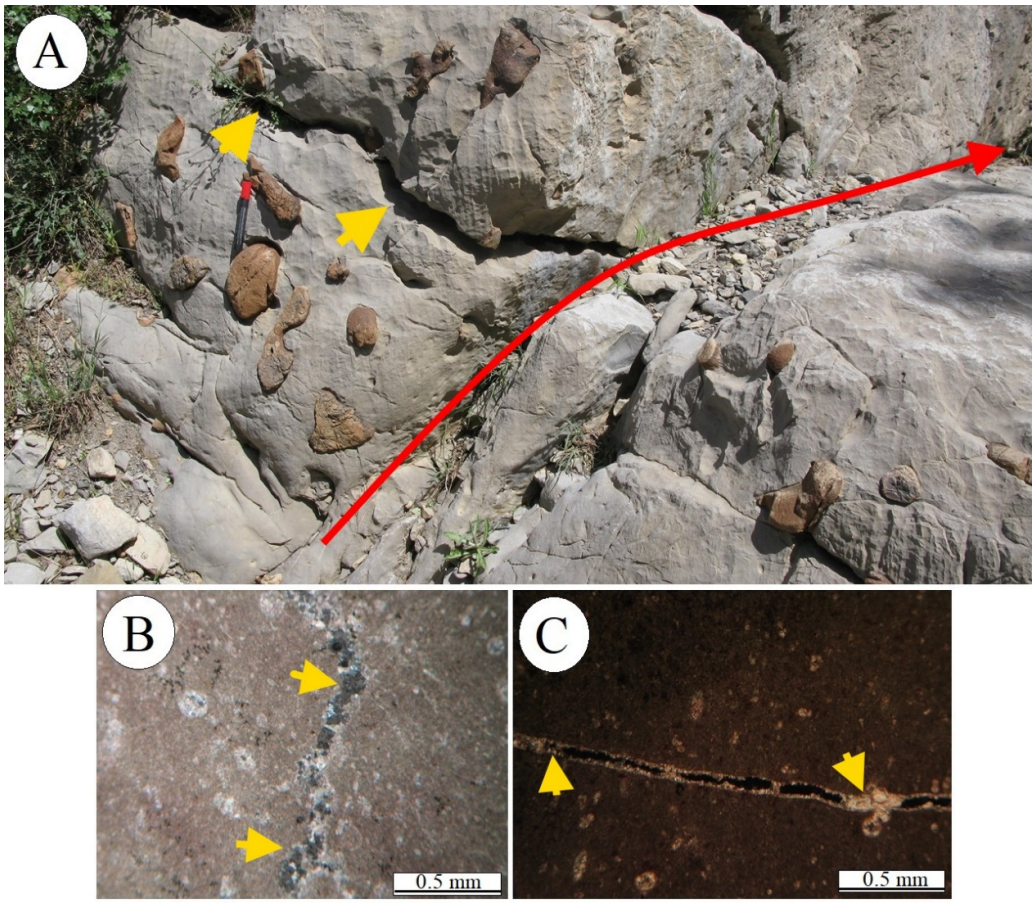


**Figure 8.** Dissolution fracture, A: in outcrop scale, B and C in thin section. The yellow arrows show the dissolution fracture and the red arrow shows the bedding plane

*Geometric parameters of the fractures*

About 752 measurements of fractures and stylolites were collected for further statistical analysis. The fracture pattern consists of two sets with approximately orientations of N120°E and N40°E in the Kuh-e-Charmi section (Fig. 4A) and N140°E and N50°E in the Surgah section (Fig. 4B) which are perpendicular to the bedding plane.

The fracture height was measured as the intersection between the fracture plane and the outcrop surface. Therefore, the value represents the minimum possible vertical extension of the fracture. Accordingly, 38 fractures have more than 500cm height, while height of the most of the fractures is less than 120cm (Figs. 9A and B).

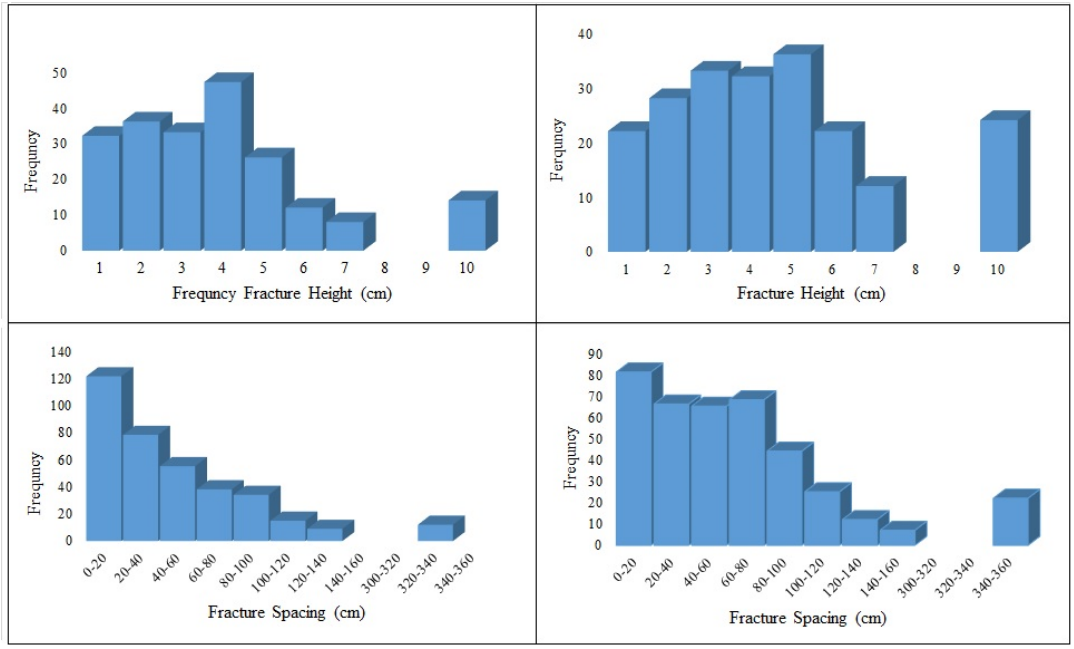


**Figure 9.** Bar chart of the fracture's geometric parameters, A and B the fractures height vs. frequency in Kuh-e-Charmi and Surgah anticline respectively, C and D: fractures spacing vs. frequency in Kuh-e-Charmi and Surgah anticline respectively

The fracture spacing was measured as perpendicular distance between two fractures of the same set. The range of fracture spacing varies between 10 and 360cm, but spacing of less than 100cm is more common (Figs. 9 C and D). In general, in both of the sections, two fracture sets were identified that are perpendicular or nearly perpendicular to the bedding plane.

Spatial distribution of fractures is controlled by several parameters including lithology, facies, early diagenesis and relationship of mechanical units with tectonic structures (Ahmadahdi et al., 2008; Barbier et al., 2012; Pireh et al., 2015). Among them, facies are the main factors controlling fracture density and spatial distribution, and their association with porosity. Furthermore, early diagenesis controls the distribution of mechanical properties of a sedimentary sequence (Barbier et al., 2012). Indeed, cement proportion can also affect the rock's mechanical properties namely tensile strength, elasticity and brittleness (Rijken, 2005).

Fractures are significantly dependent on the thickness and lithology of the layers (McClay, 1987). Layer thickness is inversely correlated by the fracture density (e.g., Underwood et al., 2003), in general, the thicker the layer, the lower the fracture density. Increasing the strength and decreasing the flexibility of the rock could lead to more closer fractures (Nelson, 2001). The lithology of the upper part of the Sarvak Formation in the study area is mainly limestone including mudstone, wackestone, packstone and grainstone facies (Esfandyari et al., 2023). The density of fractures along with lithology, texture and bed thickness in each of the inspected surface sections are given in Table 1.

In the two studied sections, longer fractures are more prominent in the coarse grain facies. The length of fractures systematically increases from mudstone to wackestone, wackestone to packstone, and packstone to grainstone (Fig. 10). Evidently, increasing the grain size causes longer fractures.

*Diagenetic sequence*

Interpretation of diagenesis and deducing the paragenetic sequence can facilitate a better understanding of the petrophysical attributes of a reservoir.

**Table 1.** Fracture parameters of the study sections

| Outcrop section | Formation | Mean bed thickness (cm) | Texture | Lithology | Fracture density (spacing) (Fr/m) |
|---|---|---|---|---|---|
| ***Surgah anticline*** | Sarvak | 25 | M | L, M | 24.3 |
| | | 35 | W | L | 11.6 |
| | | 50 | P | L | 5.8 |
| | | 75 | G | L | 3.7 |
| ***Kuh-e-Charmi*** | | 20 | M | L, M | 15.8 |
| | | 40 | W | L | 7.9 |
| | | 80 | P | L | 5.6 |
| | | 150 | G | L | 3.9 |

*Texture; M: mudstone, W: wackestone, P: packstone, G: grainstone Lithology; L: limestone, M: marl

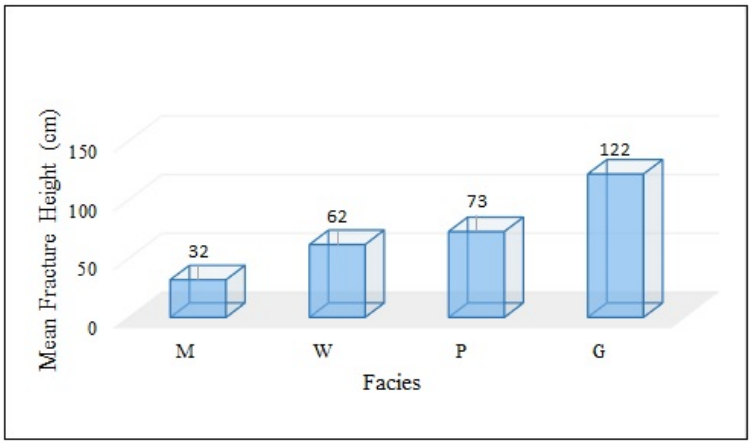


**Figure 10.** Bar chart of the fracture's height vs. facies of the Sarvak Formation. M=mudstone, W=wackestone, P=packstone, G=grainstone

Thin-section petrography and field observations were used to inspect the diagenetic processes, that revealed a wide spectrum of diagenetic processes including micritization, neomorphism, dissolution, physical compaction, fracturing, pressure solution, and cementation (Fig. 11).

Micritization

Micritization can partially or completely convert the margins of a grain or the entire grain and/or the constituents of a facies into micrite that could obliterate the original texture. Benthic foraminifera, rudist and echinoderm fragments, bivalves, and gastropods are among the skeletal constituents that were selectively micritized (Fig. 12A). In some cases, extensive micritization overprinted the original internal structure of skeletal and/or non-skeletal grains and transformed them into peloids with no relic of their original structure. This process occurs during the early stage of eogenesis (Bathurst, 1975; Tucker et al., 1990).

Neomorphism

This is mostly limited to the mudstone-wackestone-packstone facies, and caused the transformation of micrite to microspar and coarsening of the crystal size (Fig. 12B). A meteoric and/or burial realm is plausible for neomorphism.

Dissolution

Allochems were often dissolved out and left intergranular and intragranular (hybrid) pore spaces. Dissolution vugs are sub-spherical or irregular in shape, and are up to several millimeters wide.

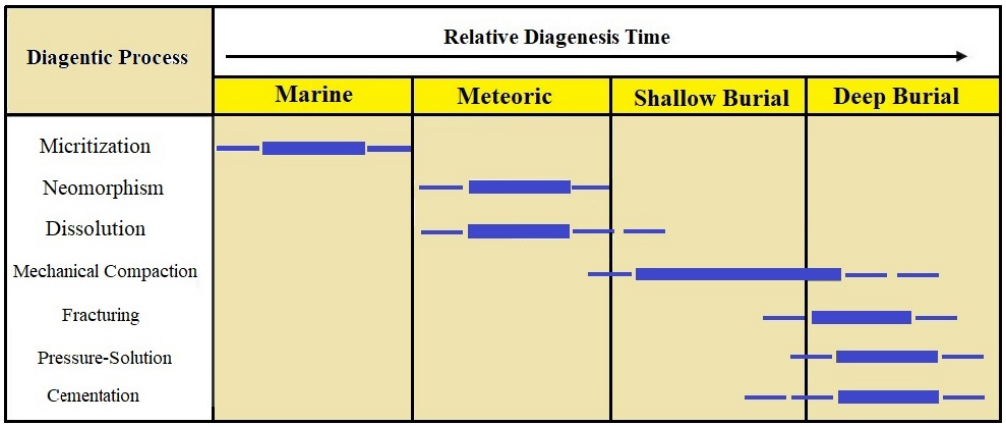


**Figure 11.** Paragenetic sequence of the diagenesis processes of the Sarvak Formation in the studied area

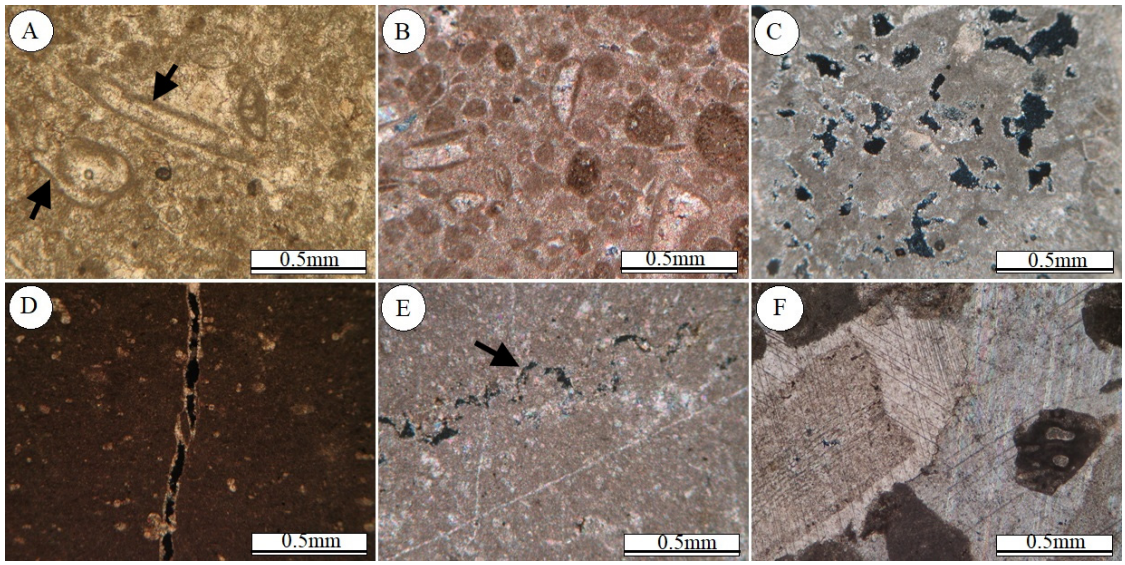


**Figure 12.** Thin section photomicrographs illustrating the diagenetic process in the Sarvak Formation, A: micritization and micrite envelop (black arrow), B: neomorphism, C: dissolution, D: fracture, E: pressure-solution and F: overgrowth rim cement around an echinoid grain and large blocky pore filling calcite spar

The vugs were partially or completely filled with calcite at the earlier stage (Fig. 12C), whereas the persisted open pores were likely filled during the burial stage.

Fracture

Some of the observed fractures were filled with coarse and blocky calcite spar, which were most likely deposited during the burial stage. In some cases, the fractures are still open and share their porosity with the formation (Fig. 12D).

Compaction

Physical compaction is common in the grain-supported facies, while it shares with chemical compaction in the mud-supported facies. Physical compaction significantly reduced the primary intergranular porosity of the grain-supported facies, which is evident from rearrangement and breakdown of brittle grains.

Stylolites were developed in both grain-supported and mud-supported facies. Dissolution seams and stylolites are evidences of chemical compaction (Fig. 12E). They are associated with compressional or shear strains during burial stage. They attest reduce in the volume of the succession and may appear as parallel and/or sub-parallel to the bedding plane (compactional strain) (McClay,1987).

Cementation

The calcite spar is common (Fig. 12F) and resembles as transparent passive void filling of the biomoldic porosity and the fractures. The large size (> 0.5mm) inclusion free crystals, imply that they were most likely precipitated during the burial stage. Chemical compaction was presumably the supplying mechanism that provided the necessary carbonate ions for the precipitation of calcite from local orogin. Primary dissolution by undersaturated fluids could incorporate the calcite into pore waters. This fluid gradually would be supersaturated and thus play a significant role to precipitate the calcite spar that passively occluded the preexisting pore spaces.

*Petrophysical characteristics*

The cross-plot of porosity versus sonic P-wave velocity ($V_p$) is shown in Fig. 13 and their numerical values are given in Table 2. The measured helium porosity values of the samples have an average of 2.01% and a variation range of 0.13-8.18%. The $V_p$ values of the samples are high, with an average of 6311 m/s and the variation range is 5488-6531 m/s. The cross-plot of $V_p$ versus porosity shows a negative linear trend in which P-wave velocity decreases with increasing porosity. In the ancient carbonates, sonic P-wave velocity is dependent on the porosity and pore types, with an inverse porosity/sonic velocity correlation (Eberli et al., 2003). Petrographic observations on the thin sections revealed different pore types in the Sarvak Formation (Fig. 14), which include microporosity, intergranular, moldic and fracture-stylolite related porosities (Table 2).

**Discussion**

In order to unravel how the diagenesis and depositional facies may have controlled the fracture development during burial stage, attempts were made to figure out the diagenetic sequence and relationships between the fractures and the physical characteristics of the country rocks.

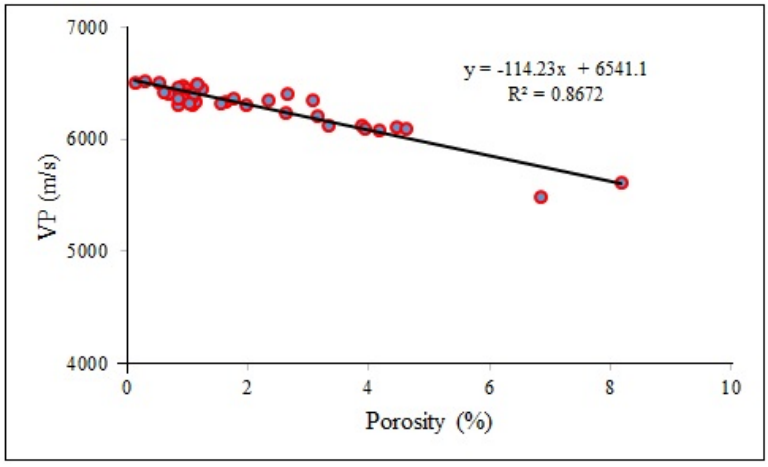


**Figure 13.** Cross-plot of porosity versus sonic P-wave velocity for the Sarvak Formation

The partially open fractures (either due to diagenetic precipitation of sparry calcite or later opening due to tectonic forces); have a considerable control on the permeability of carbonate reservoirs (Van der Voet et al., 2020).

**Table 2.** The measured petrophysical parameters of the Sarvak Formation including the porosity, P wave velocity and observed pore types

| Sample No. | Facies | Porosity (%) | P- Wave Velocity (m/s) | Pore Type |
|---|---|---|---|---|
| **H-54** | Mudstone | 1.97 | 6317 | Microporosity+ Moldic |
| **H-58** | Mudstone | 0.9 | 6468 | Microporosity+ Moldic |
| **S-8** | Mudstone | 6.85 | 5488 | Microporosity |
| **T-96** | Mudstone | 0.91 | 6487 | Microporosity+ Fracture |
| **T-97** | Mudstone | 1.22 | 6452 | Microporosity+ Stylolite |
| **T-118** | Mudstone | 1.14 | 6503 | Microporosity+ Vuggy |
| **H-15** | Wackestone | 1.04 | 6357 | Moldic |
| **H-24** | Wackestone | 1.08 | 6321 | Moldic |
| **R-1** | Wackestone | 0.97 | 6459 | Moldic |
| **S-18** | Wackestone | 1.63 | 6346 | Moldic |
| **H-1** | Packstone | 2.64 | 6408 | Moldic |
| **H-18** | Packstone | 1.13 | 6341 | Moldic+ Fracture |
| **H-22** | Packstone | 3.06 | 6363 | Moldic |
| **B-8** | Packstone | 1.75 | 6370 | Microporosity+ Moldic |
| **B-11** | Packstone | 0.94 | 6411 | Microporosity+ Moldic |
| **B-13** | Packstone | 1.07 | 6388 | Microporosity+ Moldic |
| **B-23** | Packstone | 2.34 | 6354 | Intergranular macropores |
| **A-15** | Grainstone | 4.44 | 6112 | Intergranular macropores |
| **A-25** | Grainstone | 8.18 | 5614 | Intergranular macropores |
| **A-26** | Grainstone | 3.87 | 6132 | Intergranular macropores |
| **B-9** | Grainstone | 3.93 | 6101 | Intergranular macropores |
| **B-15** | Grainstone | 3.32 | 6126 | Intergranular macropores |
| **B-23** | Grainstone | 4.17 | 6082 | Intergranular macropores |
| **B-26** | Grainstone | 1.04 | 6413 | Microporosity+ Moldic |
| **T-84** | Grainstone | 0.13 | 6509 | Microporosity+ Moldic |
| **T-120** | Grainstone | 0.69 | 6407 | Microporosity |
| **B-29** | Grainstone | 4.61 | 6096 | Microporosity+ Fracture |
| **B-25** | Grainstone | 0.61 | 6435 | Microporosity+ Stylolite |
| **T-121** | Grainstone | 0.83 | 6468 | Microporosity+ Vuggy |
| **U-97** | Grainstone | 0.84 | 6313 | Moldic |
| **T-R** | Floatstone | 1.11 | 6411 | Moldic |
| **T-9a** | Packstone | 0.91 | 6371 | Moldic |
| **T-64** | Packstone | 0.83 | 6365 | Moldic |
| **T-75** | Packstone | 2.61 | 6243 | Moldic |
| **T-21p** | Packstone | 1.54 | 6331 | Moldic+ Fracture |
| **Ku-2** | Packstone | 1.03 | 6332 | Moldic |
| **T-47** | Wackestone | 1.16 | 6501 | Microporosity+ Moldic |
| **T-83** | Wackestone | 0.28 | 6531 | Microporosity+ Moldic |
| **T-86** | Wackestone | 3.13 | 6222 | Microporosity+ Moldic |
| **T-94** | Wackestone | 0.53 | 6510 | Intergranular macropores |

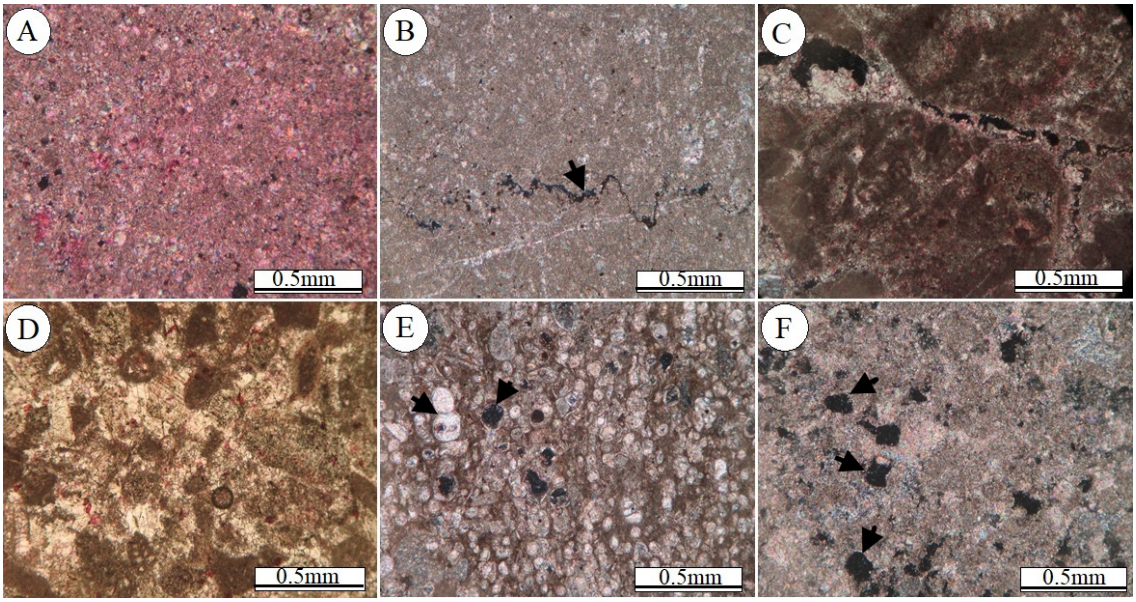


**Figure 14.** Thin section photomicrographs illustrating the main pore types in the Sarvak Formation, A: microporosity, B: stylolite porosity (black arrow); C: fracture porosity, D: tight sample in which the porosities are filled with calcite spar); E: Biomoldic porosity either filled or left open (black arrows), F: Vuggy porosity (black arrows)

To inspect the possible effect of diagenesis on the rock mechanics, the diagenetic sequence and petrophysical characteristics were examined. Petrophysical measurements show that the samples have low porosity (74% of the measured samples have only less than 3% porosity) and high $V_p$ (96% of the samples more than 6000 m/s, Table 2). Therefore, the carbonates of the Sarvak Formation can be classified as "tight". The paragenetic sequence (Fig. 11), revealed evidences of early to burial diagenetic history, during which the fracture sets and the stylolites were developed. In general, carbonates are prone to early and rapid diagenetic alteration (Anselmetti and Eberli, 1993) that makes them susceptible to the development of brittle deformation (i.e., fracturing) during later stages.

Fine-grained carbonates with large specific surface area most likely promoted the precipitation of early calcite cements in the early stages of burial (*sensu* Lavenu et al., 2015). Early cementation could increase the stiffness of rocks (Eberli et al., 2003). Rocks with low porosity are susceptible to brittle fractures and pressure solution (Rustichelli et al., 2012). In the studied carbonates, micritic matrix and early cements filled the pore spaces and reduced the original porosity, that possibly enhanced the rock mechanical strength. The studied carbonates have low porosity and high micrite matrix and a frequent fracture-stylolite were observed on the logged outcrop sections. Therefore, high content of micrite and the filling of fractures by calcite, presumably increased the bulk density of the rocks, consequently increased the P wave interval transit time, which is well documented by high $V_p$ measured in the studied samples.

The fracture pattern depends on the mechanical properties of the host rock at the time of fracturing and also on the pre-fracturing diagenetic events (Lavenu et al., 2013, 2015). The Sarvak Formation consists of carbonate facies with 0.2 to 1.4m average bed thickness. In the outcrops, fractures and stylolites are perpendicular to each other and the bedding-parallel stylolites cut across those tectonic fractures that are perpendicular to the bedding plane (Fig. 15). Thus, it is reasonable to conclude that the stylolites of the Sarvak Formation postdate the bedding-perpendicular fractures with NE-SW, and NW-SE trend.

The fractures might have originated after tectonic events, and are related to the maximum compressive $\sigma_1$ and weak differentiated extensional $\sigma_2$ and $\sigma_3$, which is well demonstrated by the simple geometry of two perpendicular fractures sets.

**Figure 15.** Bedding plane of the Sarvak Formation shows the cross-cutting relationship between the stylolites (black arrows) and bedding-perpendicular veins (red dotted lines) and fractures.

During bed parallel shortening, the maximum compressive stress ($\sigma_1$) was oriented nearly parallel to the bedding plane and perpendicular to the main trend of the Zagros fold and belt, whereas the minimum compressive stress ($\sigma_3$) might be either parallel to bedding and/or to the main trend of the Zagros belt (Tavani et al., 2018).

Tectonics stylolites may form at high angles to bedding planes during folding and indicate a layer-parallel shortening. Stylolites could normally develop perpendicular to $\sigma 1$ (Ameen et al., 2010). The observed fractures are perpendicular to the bedding plane, whilst most of the stylolites are parallel to the bedding plane. Hence, the fractures correspond to the maximum stress $\sigma_1$.

Arabia-Eurasia convergence commenced in the Late Cretaceous, caused the development of a NW-SE elongated foredeep basin (Homke et al., 2009; Saura et al., 2015). NE-SW and NW-SE trending structures were developed during this stage in the Cretaceous strata, due to the foreland flexure and along-foredeep stretching (Quintà and Tavani, 2012) from Maastrichtian to Eocene, Miocene and Pliocene in the Lurestan (Cassini et al., 2011).

## Conclusions

Genetic types of the natural fractures including tectonic, pressure-solution, and dissolution fractures were identified in the Sarvak Formation, among which the tectonic fractures are the dominant type. These fractures include two sets with NE–SW and NW–SE trends and are mostly perpendicular or nearly perpendicular to the bedding plane. Macroscopic fractures vary in height and length from several centimeters to a few meters, with a wide range of densities. Diagenetic stylolites (bedding plane parallel) and tectonic stylolites (perpendicular to bedding plane) were also observed. The fracture density is inversely correlated with the bed thickness. The fracture density and spatial distribution were mainly controlled by facies types. Height of the fractures are inversely correlated mud matrix content of the facies. Shift from mud-supported to grain-supported texture caused the development of much longer fractures. There is also a direct correlation between grain size and the fracture's height. Indeed, the depositional

facies controls the initial mechanical properties and susceptibility to the diagenetic processes. Petrophysical measurements revealed that the carbonates of the Sarvak Formation could be classified as tight carbonates. Helium porosity and Vp values have an average of 2.01% 6311 m/s respectively. The P-wave velocity and porosity are inversely correlated.
The outcomes of the present study provide a key framework for a better understanding of the fracture development and spatial distribution in the Sarvak carbonate reservoir and its analogues elsewhere in the Zagros Basin.

## Acknowledgement

This research was funded by a grant to H. Mohseni via Vice-president Research Affair of Bu-Ali Sina University. The authors would like to thanks to the anonymous reviewers of Geopersia for their critical review and constructive comments.

## References

Agard, P., Omrani, J., Jolivet, L., Mouthereau, F., 2005. Convergence history across Zagros, Iran; constraints from collisional and earlier deformation, Geologische Rundschau, International Journal Earth Sciences 94: 401-419.

Ahmadahdi, F., Daniel, J.M., Azzizadeh, M., Lacombe, O., 2008. Evidence for prefolding vein development in the Oligo-Miocene Asmari formation in the central Zagros fold-belt, Iran. Tectonics 27: TC1016.

Ahmadhadi, F., Daniel, J.-M., Azzizadeh, M., Lacombe, O., 2008. Evidence for pre-folding vein development in the Oligo-Miocene Asmari Formation in the Central Zagros Fold Belt. Iran. Tectonics 27: TC1016.

Alavi, M., 1991. Sedimentary and structural characteristics of the Paleo-Tethys remnant in NE Iran. Geological Society of America Bulletin 103: 983-992.

Alavi, M., 2007. Structures of the Zagros fold-thrust belt in Iran. American Journal of Science 307: 1064-1095.

Alsharhan, A., Sadd, J.L., 2000. Stylolites in Lower Cretaceous Carbonate Reservoirs 69. Society for Sedimentary Geology Special Publication, U.A.E: 185-207pp.

Angerer, E., Lanfranchi, P., Rogers, S.F., 2003. Fractured reservoir modeling from seismic to simulator: A reality? The Leading Edge 22 (7): 684-689.

Awdal, A.H., Braathen, A., Wennberg, O.P., Sherwani, G.H., 2013. The characteristics of fracture networks in the Shiranish Formation of the Bina Bawi Anticline; comparison with the Taq Taq Field, Zagros, Kurdistan, NE Iraq. Petroleum Geosciences 19: 139.155.

Aydin, A., 2000. Fractures, faults, and hydrocarbon entrapment, migration and flow. Marine and Petroleum Geology 17(7): 797-814.

Barbier, M., Hamon, Y., Callot, J.P., Floquet, M., Daniel, J.M., 2012. Sedimentary and diagenetic controls on the multiscale fracturing pattern of a carbonate reservoir: The Madison Formation (Sheep Mountain, Wyoming, USA). Marine and Petroleum Geology 29: 50-67.

Beaudoin, N., Koehn, D., Lacombe, O., Lecouty, A., Billi, A., Aharonov, E., Parlangeau, C., 2016. Fingerprinting stress: stylolite and calcite twinning paleopiezometry revealing the complexity of progressive stress patterns during folding-the case of the Monte Nero anticline in the Apennines, Italy. Tectonics 35:1687-1712.

Berberian, M., 1995. Master 'blind' thrust faults hidden under the Zagros folds: Active basement tectonics and surface morphotectonics, Tectonophysics 241, 3-4: 193-224.

Berberian, M., King, G.C.P., 1981. Towards a paleogeography and tectonic evolution of Iran. Canadian Journal of Earth Sciences 18: 210-265.

Birch, F., 1960. The velocity of compressional waves in rocks to 10 kilobars: 1. Geophysical Research 65: 1083-1102.

Bordenave, M.L., 2008. The origin of the permo- triassic gas accumulations in the Iranian Zagros fold belt and contiguous offshore areas: a review of the Paleozoic petroleum system. Petroleum Geology

31: 3-42.
Carminati, E., Aldega, L., Bigi, S., Corrado, S., D'Ambrogi, C., Mohammadi, P., Shaban, A., Sherkati, S., 2013. Control of Cambrian evaporites on fracturing in fault-related anticlines in the Zagros fold-and-thrust belt. International Journal Earth Sciences 102: 1237-1255.
Carminati, E., Aldega, L., Trippetta, F., Shaban, A., Narimani, H., Sherkati, S., 2014. Control of folding and faulting on fracturing in the Zagros (Iran): The Kuh-e-Sarbalesh anticline. Asian Earth Sciences 79: 400-414.
Casciello, E., Verges, J., Saura, E., Casini, G., Fernandez, N., Blanc, E., Homke, S., Hunt, D.W., 2009. Fold patterns and multilayer rheology of the Lurestan Province, Zagros Simply Folded Belt (Iran). Geological Society 166: 947-959.
Casini, G., Gillespie, P.A., Vergés, J., Romaire, I., Fernandez, N., Casciello, E., Saura, E., Mehl, C., Homke, S., Embry, J. C., Aghajari, L., Hunt, D.W., 2011. Sub-seismic fractures in foreland fold and thrust belts: insight from the Lurestan Province, Zagros Mountains, Iran. Petroleum Geosciences 17: 263-282.
Cooper, M., 2007. Structural style and hydrocarbon prospectivity in fold and thrust belts: a global review. Special Publication-Geological Society of London 272: 447pp.
Dunham, J.B.; Larter, S. 1981. Association of Stylolitic Carbonates and Organic Matter: Implications for Temperature Control on Stylolite Formation. American Association of Petroleum Geologists 65: 922.
Eberli, G.P., Baechle, G.T., Anselmetti, F.S., Incze, M.L., 2003. Factors controlling elastic properties in carbonate sediments and rocks. The Leading Edge 22 (7): 654-660.
Ebner, M., Toussaint, R., Schmittbuhl, J., Koehn, D., Bons, P., 2010. Anisotropic scaling of tectonic stylolites: a fossilized signature of the stress field. Geophys. Research: Solid Earth 115, 6: B06403.
Esfandyari, M., Mohseni, H., Heidari, M., 2023. Facies analysis, depositional sequences and platform evolution of the Sarvak Formation (late Albian-Turonian) in the Zagros Basin, West of Iran. African Earth Sciences 198: 104811.
Falcon, N. L., 1961. Major earth-flexuring in the Zagros mountains of south-west Iran, Geological Society, London 117(468): 367-376.
Falcon, N.L., 1974. Southern Iran: Zagros Mountains. Geological Society, London, Special Publications 4(1): 199-211.
Farzipour-Saein, A., Yassaghi, A., Sherkati, S., Koyi, H., 2009. Basin evolution of the Lurestan region in the Zagros Fold-and-Thrust Belt, Iran. Petroleum Geology 32, 1: 5-20.
Heydari, E., 2008. Tectonics versus eustatic control on supersequences of the Zagros Mountains of Iran, Tectonophysics, 451 (1–4), 56-70.
Homke, S., Verges, J., Serra-Kiel, J., Bernaola, G., Sharp, I., Garces, M., Montero- Verdu, I., Karpuz, R., Goodarzi, M.H., 2009. Late Cretaceous- Paleocene formation of the proto- Zagros foreland basin, Lurestan Province, SW Iran Geological Society of America Bulletin 121; 7-8: 963-978.
Koehn, D., Rood, M.P., Beaudoin, N., Chung, P., Bons, P.D., Gomez-Rivas, E., 2016. A new stylolite classification scheme to estimate compaction and local permeability variations. Sedimentary Geology, 346: 60-71.
Kordi, M., 2019. Sedimentary basin analysis of the Neo-Tethys and its hydrocarbon systems in the Southern Zagros fold-thrust belt and foreland basin. Earth-Science Reviews 191: 1-11.
Kosari, E., Kadkhodaie, A., Bahroudid, A., Chehrazie, A., Talebiana, M., 2017. An integrated approach to study the impact of fractures distribution on the Ilam-Sarvak carbonate reservoirs: A case study from the Strait of Hormuz, the Persian Gulf. Petroleum Science and Engineering 152: 104-115.
Lavenu, A.P.C., Lamarche, J., Gallois, A., Gauthier, B.D.M., 2013. Tectonic versus diagenetic origin of fractures in naturally fractured carbonate reservoir analogue: The Nerthe anticline (southeastern France). American Association of Petroleum Geologists 97 (12): 2207-2232.
Lavenu, A.P.C., Lamarche, J., Texier, L., Marie, L., Gauthier, B.D.M., 2015. Background fractures in carbonates: inference on control of sedimentary facies, diagenesis and petrophysics on rock mechanical behavior. Example of the Murge Plateau (southern Italy). Ital. Geosciences 134 (3): 535-555.
Lee, H., Lee, S.G., Doyle, P.S., 2015. Photo patterned oil-reservoir micromodels with tailored wetting properties. Lab on a Chip 15(14): 3047-3055.
Li, J.; Zeng, L.; Li, W.; Zhang, Y.; Cai, Z., 2019. Controls of the Himalayan deformation on hydrocarbon

accumulation in the western Qaidam Basin, Northwest China. China. Asian Earth Sciences 174: 294-310.
Liu, G., Zeng, L., Han, C., Ostadhassan, M., Lyu, w., Wang, Q., Zhu, J., Hou, F., 2020. Natural Fractures in Carbonate Basement Reservoirs of the Jizhong Sub-Basin, Bohai Bay Basin, China: Key Aspects Favoring Oil Production. Energies 13: 4635.
Lynn, H.B., 2004. The winds of change, anisotropic rocks- their preferred direction of fluid flow and their associated seismic signatures- part 1. The Leading Edge 23: 1156-1162.
McClay, K.R., 1987.The mapping of geological structures, Geological Society of London Handbook: 161pp.
McClusky, S., Reilinger, R., Mahmoud, S., Ben Sari, D., Tealeb, A., 2003. GPS constraints on Africa (Nubia) and Arabia plate motions, Geophysical Journal International 155 (1): 126-138.
Motiei, H., 1993. Stratigraphy of Zagros. Geological Survey of Iran, Tehran: 536 pp.
Nelson, R.A., 1981. Significance of fracture sets associated with stylolite zones. American Association of Petroleum Geologists 65 (11): 2417-2425.
Nelson, R.A., 2001. Geological analysis of naturally fractured reservoirs. Houston, Gulf Professional Publishing, 2nd edition: 332 pp.
Peacock, D.C.P., 2006. Predicting variability in joint frequencies from boreholes. Structural Geology 28 (2): 353-361.
Petit, J.P., Mattauer, M., 1995. Paleostress superimposition deduced from meso-scale structures in limestone- the matellese exposure, Languedoc. France. Structural Geology 17: 245-256.
Pireh, A., Alavi, S.A., Ghassemi, M.R., Shaban, A., 2015. Analysis of natural fractures and effect of deformation intensity on fracture density in Garau formation for shale gas development within two anticlines of Zagros fold and thrust belt, Iran. Petroleum Science and Engineering 125: 162-180.
Quintà, A., Tavani, S., 2012. The foreland deformation in the south-western Basque- Cantabrian Belt (Spain). Tectonophysics 576-577: 4-19.
Rijken, P., 2005. Modeling naturally fractured reservoirs: from experimental rock mechanics to flow simulation. Ph.D. dissertation, University of Texas at Austin, Austin, Texas: 239p.
Rustichelli, A., Tondi, E., Agosta, F., Cilona, A., Giorgioni, M., 2012. Development and distribution of bed-parallel compaction bands and pressure solution seams in carbonates (Bolognano Formation, Majella Mountain, Italy). Structural Geology, 37: 181-199.
Saura, E., Garcia-Castellanos, D., Casciello, E., Parravano, V., Urruela, A., Vergés, J., 2015. Modeling the flexural evolution of the Amiran and Mesopotamian foreland basins of NW Zagros (Iran-Iraq). Tectonics 34: 377-395.
Setudehnia, A., 1978. The Mesozoic sequence in Southwest Iran and adjacent areas. Petroleum Geology 1: 3-42.
Tavani, S., Corradetti, A., Sabbatino, M., Morsalnejad, D., Mazzoli, S., 2018. The Meso-Cenozoic fracture pattern of the Lurestan region, Iran: The role of rifting, convergence, and differential compaction in the development of pre-orogenic oblique fractures in the Zagros Belt. Tectonophysics 749 :104-119.
Tavani, S., Storti, F., Lacombe, O., Corradetti, A., Muñoz, J.A., Mazzoli, S., 2015. A review of deformation pattern templates in foreland basin systems and fold and thrust belts: Implications for the state of stress in the frontal regions of thrust wedges. Earth- Science Review 141: 82-104.
Terzaghi, R.D., 1965. Source of error in joint surveys. Géotechnique 15(3): 287-304.
Underwood, C.A., Cooke, M.L., Simo, J.A., Muldoon, M.A., 2003. Stratigraphic controls on vertical fracture patterns in Silurian dolomite, northeastern Wisconsin. American Association of Petroleum Geologists 87(1):121–142.
Van der Voet, E., Muchez, P., Laenen, B., Weltje, G.J., Lagrou, D., Swennen, R. 2020. Characterizing carbonate reservoir fracturing from borehole data – A case study of the Viséan in northern Belgium, Marine and Petroleum Geology, 111: 375-389.
Verges, J., Saura, E., Casciello, E., Fernàndez, M., Villaseñor, A., Jiménez-Munt, I., García-Castellanos, D., 2011. Crustal-scale cross-sections across the NW Zagros belt: implications for the Arabian margin reconstruction. Geological Magazine 148: 739-761.
Warren, J. K. 2006. Evaporites, Sediments, Resources and Hydrocarbons, Springer-Verlag Berlin. 1035 p.
Wennberg, O.P., Azizzadeh, M., Aqrawi, A.A.M., Blanc, E., Brockbank, P., Lyslo, K.B., Pickard, N., Salem, L.D., Svana, T., 2007. The Khaviz Anticline: an outcrop analogue to giant fractured Asmari

Formation reservoirs in SW Iran. Geological Society, London, Special Publications, 270: 23-42.
Wennberg, O.P., Svana, T., Azizzadeh, M., Aqrawi, A.M.M., Brockbank, P., Lyslo, K.B., Ogilvie, S., 2006. Fracture intensity vs. mechanical stratigraphy in platform top carbonates: The Aquitanian of the Asmari Formation, Khaviz Anticline, Zagros, SW Iran. Petroleum Geosciences 12: 235-246.